Spring 1-1-2011

Regenerative Power Optimal Reaction Wheel Attitude Control

Robin M. Blenden
University of Colorado at Boulder, robin.blenden@gmail.com

Regenerative Power Optimal Reaction Wheel Attitude Control

by

R. M. Blenden

B.S., University of Colorado, 2010

A thesis submitted to the

Faculty of the Graduate School of the

University of Colorado in partial fulfillment

of the requirements for the degree of

Master of Science

Department of Aerospace Engineering Sciences

2011

This thesis entitled:
Regenerative Power Optimal Reaction Wheel Attitude Control
written by R. M. Blenden
has been approved for the Department of Aerospace Engineering Sciences

_____
Hanspeter Schaub

_____
Penina Axelrad

_____
Eric Frew

Date _____

The final copy of this thesis has been examined by the signatories, and we find that both the content and the form meet acceptable presentation standards of scholarly work in the above mentioned discipline.

Blenden, R. M. (M.S., Aerospace Engineering Sciences)

Regenerative Power Optimal Reaction Wheel Attitude Control

Thesis directed by Prof. Hanspeter Schaub

The thesis work develops an instantaneous power optimal attitude control for a spacecraft utilizing an integrated reaction wheel - flywheel system allowing for energy storage and return. The control is generally formulated to utilize an arbitrarily large number of reaction wheels, and is applicable to any system with redundant wheels spanning three-dimensional space. This is accomplished by manipulation of the wheel torque null motion such that the resulting attitude dynamics are not affected. By application of physical constraints on the wheel motor performance, the solution method to find the null torques is reduced to a hyperdimensional vector geometry problem, and the proper control torques are uniquely determined. The resulting power optimal control guarantees that the instantaneous maximum power is returned from the reaction wheels at all times. This control is then applied to a variety of control laws, demonstrating its behavior for a variety of control applications and initial spacecraft states. These include a velocity regulator control and attitude a velocity tracking control. Comparison to other relevant reaction wheel controls demonstrates the analytically developed instantaneous power optimal and minimum energy state seeking behavior. Finally, future developments are suggested, including the incorporation of wheel power return inefficiency and application of the developed methodology for integrated energy storage and power tracking.

Contents

Chapter

Figures

Figure

Chapter 1

Introduction and Literature Review

1.1 Motivation

The attitude control system is a critical component of most spacecraft, responsible for pointing antennas, solar arrays, instruments and other payloads. This can be accomplished through a variety of means to reorient the spacecraft[1]. These systems fall into two basic categories; those which generate an external torque to orient the spacecraft, and those which perform internal momentum exchange. The former includes thruster systems, which are easily implemented but must carry fuel, and magnetic systems, which use the Earth's magnetic field to align either passively or actively (these are particularly popular on small spacecraft). The latter category consist of angular momentum exchange systems, which are the focus of the work below.

Momentum exchange systems are often favored because of the pointing precision and fuel-free operation. The two commonly used momentum exchange devices are reaction wheels and control moment gyroscopes. Both systems utilize a spinning momentum wheel, the difference being that the orientation of the reaction wheel is fixed with respect to the rest of the spacecraft, while the gyroscope's orientation changes. The reaction wheel exchanges momentum with the spacecraft body by accelerating or deccelerating the wheel, changing the wheel momentum magnitude, while the control moment gyroscope reorients the wheel, changing the wheel momentum direction (variable speed control moment gyroscopes are capable of both, and have many advantages). While control moment gyroscopes have the advantage of generating larger control torques (useful for larger and more agile spacecraft), they are complex and massive compared to reaction wheels[1][2]. For this

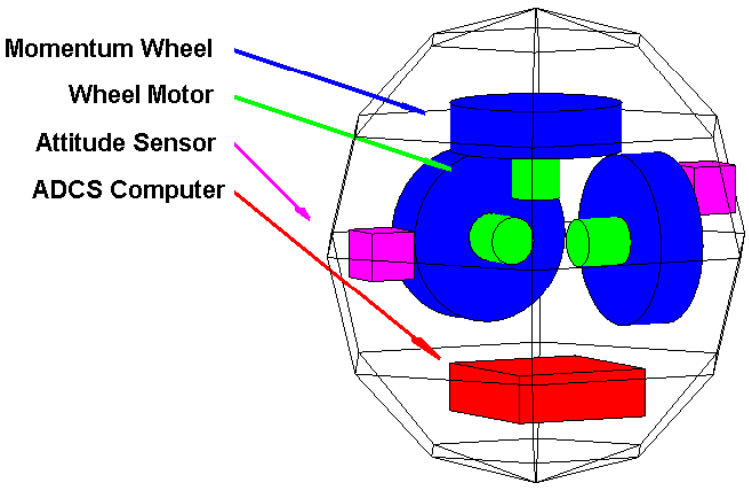

Figure 1.1: Generic Reaction Wheel Attitude Control System

reason, reaction wheels are favored for many applications.

Power is always a scarce resource on a spacecraft, and momentum exchange devices can be a considerable load[1]. While enhancing the performance of a particular subsystem generally requires designs trade-offs, optimal attitude control design can be applied to create power savings with no negative consequences. Power optimal controls are of particular relevance for small spacecraft, which are currently of great interest. Use of power optimal attitude controls systems, as well as integrated energy storage systems, can greatly increase the capability of such spacecraft in the near future[3][4].

1.2 Literature Review of Previous Power Optimal Control Research

There are many methods by which a given control goal may be achieved, allowing for substantial variation to optimize various aspects of the control performance. A common performance objective is the optimization of the attitude control system load on the power system. These power

optimal controls generally focus on minimizing the energy used over the course of an entire maneuver (see [5],[6],[7]), although some aim to instantaneously minimize the power consumption (see [8]).

Most power optimal research applicable to reaction wheel systems has focused on minimizing the average power consumption over the course of a maneuver. Since the wheel motor power is the product of the wheel speed and wheel motor torque, this can be altered by changing either variable. Some strategies achieve this goal by working directly to minimize the integral of the wheel motor power over the course of a maneuver. By applying variational methods, the optimal wheel torque trajectory can be determined numerically[5].

While these controls are useful to directly control reaction wheel torques, other power optimization strategies work indirectly. While only three reaction wheels are needed to produce a general three axis control torque, many spacecraft carry at least one additional wheel for redundancy. Based upon design considerations, some, such as the Swift spacecraft shown in Fig. (1.2), carry as many as six[9]. Due to this redundancy, there are an infinite number of wheel torque solutions to produce the same total control torque. This fact can be utilized to formulate a different set of power optimal controls for such redundant configurations.

A popular approach is to constantly minimize all wheel speeds. These controls generally work by integrating the wheel speed error with respect to a minimum value (since a zero rate may be undesirable), and adjusting the wheel torque solution to constantly drive this error to zero[10][11]. More recent research uses similar mathematical techniques to directly minimize the power consumption at any given instant. The instantaneous power optimal control strategy is distinct from the methods above, since it guarantees optimal power use at any arbitrary instant but no long term behavior. For practical applications, instantaneous and long term power optimal controls could be used in conjunction to produce the desired behavior, utilizing the best qualities of each. This instantaneous power optimal control is the basis of the work presented here, and is discussed in some detail below[8].

In addition to attitude control system power optimization, there has been considerable inter-

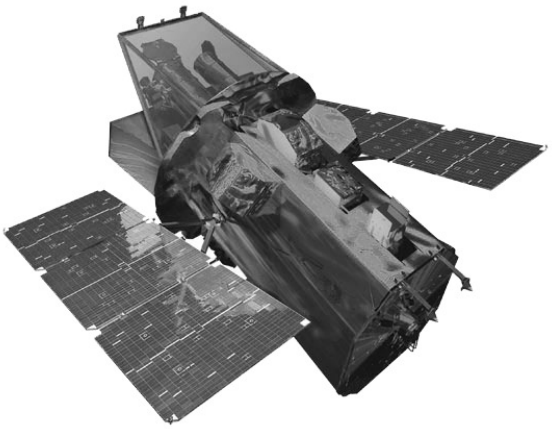

Figure 1.2: Swift Gamma-Ray Observatory[1]

est (dating to the 1960s) in incorporation of energy storage capability into commonly used attitude control systems, since the reaction wheels and variable speed control moment gyroscopes are ideal for use as flywheels. Flywheels are favorable when compared to chemical batteries for many other reasons, including extended lifetime and depth of discharge[4]. Application of integrated power and control systems (IPACS) could provide considerable spacecraft mass savings by eliminating some of the required capacity for chemical energy storage. Mechanical energy storage could provide a backup power system with no additional mass penalty, which would be of particular use during orbital eclipse and other periods of high demand on the energy storage systems. Due to dynamic constraints, flywheel systems are not generally well suited to replace chemical batteries altogether, but are useful for supplementing primary systems for power tracking and additional energy storage capacity[12][13][14]. A variety of control approaches have demonstrated the ability to simultaneously perform attitude control and useful power tracking[12]. By utilizing the redundancy of the reaction wheels, an arbitrary power profile may be tracked without interfering with the attitude control performance[4][15][16]. This is accomplished by decomposing the reaction wheel torques into two decoupled attitude control and power control components, using the same mathematical techniques as the power optimal controls above. By comparing power output against a desired power profile, this has been expanded to create a more robust power tracking feedback control

[1] illustration: http://www.lanl.gov/news/index.php/fuseaction/nb.story/story_id/\%2015738

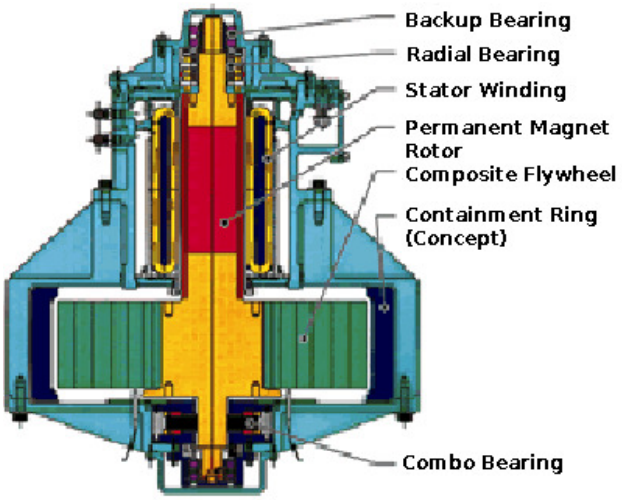

Figure 1.3: Spacecraft Flywheel Schematic[2]

law[12]. These techniques have also been applied to variable speed control moment gyroscopes, which provide an additional degree of flexibility. By adapting techniques developed for singularity avoidance using the VSCMG reaction wheel mode[2], a similar result can be achieved[2][6].

Both power optimal controls and IPACS are of particular interest when designing small spacecraft. Small spacecraft are inexpensive and versatile, and recent interest in their applications has spurred development of more advanced attitude control systems to improve their capabilities[17]. In such spacecraft (generally with a mass less the 500 kg, and sometimes as little as 1 kg), mass and power budgets are particularly strict. With such limited available power, momentum exchange systems for attitude control are difficult to implement, making instantaneous power optimal controls very important[8]. The incorporation of IPACS promises substantial mass savings (on the order of 50% for the combined power and attitude control systems), since chemical batteries generally consume a large portion of a small spacecraft's mass[18]. The work below is very relevant to small spacecraft, since it applies an IPACS-type system to produce instantaneous power optimal behavior not possible with a conventional reaction wheel system.

While spacecraft flywheel systems are a promising field of research, there are many technical challenges to be confronted. In addition to dynamics issues (such as power or attitude tracking

[2] illustration: http://soliton.ae.gatech.edu/labs/dcsl/research-ipacs.html

singularities) affecting the control strategies described above, there are many hardware related obstacles. The high speeds required (upwards of $50,000\,\text{rpm}$) are demanding of the materials selected for the wheel, and require use of composites to be feasible. The wheel bearings must also be exceptionally high performance, generally requiring magnetic bearings. IPACS and other flywheel energy storage systems are actively being developed by NASA and the USAF, among others, to tackle these challenges[15][4][12].

1.3 Thesis Goals

The work presented below derives a reaction wheel attitude control which minimizes the instantaneous total power returned by a hybrid reaction wheel - flywheel system that allows for energy return. This formulation is applicable to any such vehicle with an arbitrarily large number of redundant wheels, and can be applied to any generalized control law. The underlying mathematics are explained in detail and related to the physical behavior of the system when possible. After deriving the system dynamics and the regenerative reaction wheel control, a series of numerical maneuver simulations are presented. These demonstrate important aspects of the control's behavior for a variety of applications, comparing them to other relevant reaction wheel controls. Finally, important future developments of the work presented here are described briefly, including shortcomings and other potential applications.

Chapter 2

General Control Law Development

2.1 Definition of System

Before deriving any controls, power optimal or otherwise, it is first necessary to define the spacecraft dynamics and equations of motion. In this generalized rigid body dynamics problem, the spacecraft body fixed frame $\mathcal{B}$ is rotating with respect to the inertial frame $\mathcal{N}$. Its total angular momentum may be decomposed into the separate momenta of the static components of the spacecraft, $\mathbf{H}_b$, and its n arbitrarily oriented reaction wheels, $\mathbf{H}_s$[2].

$$\mathbf{H} = \mathbf{H}_b + \mathbf{H}_s \tag{2.1}$$

Assuming that the spacecraft may be modeled as a rigid body with inertia tensor $[I]$, a constant when given in the $\mathcal{B}$ frame, the body angular momentum $\mathbf{H}_b$ is expressed in terms of $[I]$ and the body angular velocity $\boldsymbol{\omega}$ (the $\mathcal{B}$ frame angular velocity with respect to the inertial $\mathcal{N}$ frame) as

$$\mathbf{H}_b = [I]\,\boldsymbol{\omega} \tag{2.2}$$

The inertia tensor $[I]$ is assumed to account for all inertia components except for the reaction wheel inertia about their respective spin axes. Given that each wheel is aligned along the spin axis $\hat{\mathbf{g}}_i$, the wheel inertia component $\mathbf{H}_s$ can the be expressed by projecting the vector of individual wheel momenta $\mathbf{h}_s$ into the body frame

$$\mathbf{H}_s = [G]\,\mathbf{h}_s \tag{2.3}$$

The $3 \times n$ matrix $[G]$ projects the wheel momentum and torque vectors onto the body momentum space, and is defined in terms of the wheel spin axes as

$$[G] = \left[\begin{array}{cccc} \hat{\mathbf{g}}_1 & \hat{\mathbf{g}}_2 & \cdots & \hat{\mathbf{g}}_n \end{array} \right] \tag{2.4}$$

The wheel momentum vector $\mathbf{h}$ is defined in terms of the wheel inertias J_i and spacecraft angular velocities as

$$\mathbf{h} = \left(\begin{array}{c} J_1 \left(\omega_{s,1} + \Omega_1 \right) \\ J_2 \left(\omega_{s,2} + \Omega_2 \right) \\ \vdots \\ J_n \left(\omega_{s,n} + \Omega_n \right) \end{array} \right) \tag{2.5}$$

$\omega_{s,i}$ is the component of the spacecraft angular velocity in the i^{th} wheel spin axis, defined as

$$\omega_{s,i} = \boldsymbol{\omega} \cdot \hat{\mathbf{g}}_i \tag{2.6}$$

The equations of motion are developed by finding the inertial derivative of Eqn. (2.1). Taking the derivative of Eqn. (2.2) as seen by the $\mathcal{N}$ frame via application of the transport theorem yields[2]

$$\dot{\mathbf{H}}_b = - \left[\tilde{\omega} \right] [I] \, \boldsymbol{\omega} + \mathbf{L} \tag{2.7}$$

The external torque is neglected for the developments below, so $\mathbf{L} = \mathbf{0}$. The $[\tilde{\omega}]$ is the matrix equivalent of a vector cross-product, and is defined as

$$[\tilde{\omega}] = \left[\begin{array}{ccc} 0 & -\omega_3 & \omega_2 \\ \omega_3 & 0 & -\omega_1 \\ -\omega_2 & \omega_1 & 0 \end{array} \right] \tag{2.8}$$

This notation is used to clarify the resulting mathematics, but it can be trivially shown that $[\tilde{\omega}] \, \mathbf{a} = \boldsymbol{\omega} \times \mathbf{a}$. Similarly, taking the inertial derivative of the wheel momentum vector $\mathbf{H}_s$ gives

$$\dot{\mathbf{H}}_s = - \left[\tilde{\omega} \right] [G] \, \mathbf{h}_s - [G] \, \mathbf{u} \tag{2.9}$$

The $[G]$ matrix is also used here to project the wheel motor torques onto the body frame $\mathcal{B}$. The n-dimensional wheel torque vector $\mathbf{u}$ is defined as

$$\mathbf{u} = \begin{pmatrix} u_1 \\ u_2 \\ \vdots \\ u_n \end{pmatrix} \tag{2.10}$$

Substituting Eqn. (2.7) and Eqn. (2.9) into the derivative of Eqn. (2.1) yields the following equation of motion, a reaction wheel specific form of Euler's equation

$$[I]\,\dot{\boldsymbol{\omega}} = -\,[\tilde{\omega}]\,[I]\,\boldsymbol{\omega} - [\tilde{\omega}]\,[G]\,\mathbf{h}_s - [G]\,\mathbf{u} \tag{2.11}$$

Control laws to govern angular velocity, attitude, or both can then be derived using the equation of motion given in Eqn. (2.11). The calculation of the wheel torques $\mathbf{u}$ which produce this torque is generally a distinct procedure, and is dealt with in detail below. Two feedback control laws governing the control torque $[G]\,\mathbf{u}$, which are implemented in the numerical simulations, are derived below.

2.2 Velocity Regulator Control

The first control is a basic detumbling velocity regulator control, which drives the body angular velocity to zero. In order for the system to be guaranteed globally stable about a desired state, a continuously differentiable, positive definite, negative semidefinite Lyupanov function must exist for the system. To begin, the spacecraft kinetic energy (excluding the reaction wheels) is chosen as a possible Lyupanov function V

$$V = \frac{1}{2}\boldsymbol{\omega}^T\,[I]\,\boldsymbol{\omega} \tag{2.12}$$

This is an excellent candidate, since it is positive definite in terms of the angular velocity for any inertia tensor $[I]$. Taking the time derivative of this function gives

$$\dot{V} = \boldsymbol{\omega}^T\,[I]\,\dot{\boldsymbol{\omega}} \tag{2.13}$$

Substituting Eqns. (2.11) and (3.1) yield the following expression for the Lyupanov function derivative, which now incorporates the system dynamics.

$$\dot{V} = \boldsymbol{\omega}^T \left(- \left[\tilde{\omega}\right] \left[I\right] \boldsymbol{\omega} - \left[\tilde{\omega}\right] \left[G\right] \mathbf{h}_s - \left[G\right] \mathbf{u} \right) \tag{2.14}$$

In order to guarantee that Eqn. (2.14) is negative semidefinite it is set equal to

$$\dot{V} = -P \boldsymbol{\omega}^T \boldsymbol{\omega} \tag{2.15}$$

P is a scalar feedback gain, which must be positive. Substituting the control into Eqn. (2.13) and solving for the control torque $\left[G\right] \mathbf{u}$ yields the following regulator control law

$$\left[G\right] \mathbf{u} = P\boldsymbol{\omega} - \left[\tilde{\omega}\right] \left(\left[I\right] \boldsymbol{\omega} + \left[G\right] \mathbf{h}_s \right) \tag{2.16}$$

This simple control guarantees that the spacecraft body angular velocity will always approach zero with respect to the inertial frame.

2.3 Attitude and Velocity Tracking Control

The other control implemented below is more general, and capable of tracking the angular velocity and attitude history of a reference frame $\mathcal{R}$. The inertial frame $\mathcal{N}\left\{\hat{\mathbf{n}}_1, \hat{\mathbf{n}}_2, \hat{\mathbf{n}}_3\right\}$, body frame $\mathcal{B}\left\{\hat{\mathbf{b}}_1, \hat{\mathbf{b}}_2, \hat{\mathbf{b}}_3\right\}$, and reference frame $\mathcal{R}\left\{\hat{\mathbf{r}}_1, \hat{\mathbf{r}}_2, \hat{\mathbf{r}}_3\right\}$ are shown in Fig. (2.1). The body frame attitude is given by the modified Rodrigues parameter (MRP) vector $\boldsymbol{\sigma}$ (actually just a 3×1 matrix), while the reference frame attitude is given by $\boldsymbol{\sigma}_r$. The body frame and reference frame angular velocities with respect to the inertial frame are $\boldsymbol{\omega}$ and $\boldsymbol{\omega}_r$, respectively.

The difference in the attitude of the $\mathcal{B}$ frame and the $\mathcal{R}$ frame is defined by attitude error vector $\boldsymbol{\sigma}_\delta$. The MRP sets do not constitute a vector space, so they cannot be vectorially added or subtracted like the angular velocities. However, a subtraction formula can be derived by relating their resulting rotation matrices, and is directly expressed as[2]

$$\boldsymbol{\sigma}_\delta = \frac{\left(1 - \left|\boldsymbol{\sigma}_r\right|^2\right) \boldsymbol{\sigma} - \left(1 - \left|\boldsymbol{\sigma}\right|^2\right) \boldsymbol{\sigma}_r + 2\boldsymbol{\sigma} \times \boldsymbol{\sigma}_r}{1 + \left|\boldsymbol{\sigma}_r\right|^2 \left|\boldsymbol{\sigma}\right|^2 + 2\boldsymbol{\sigma}_r \cdot \boldsymbol{\sigma}} \tag{2.17}$$

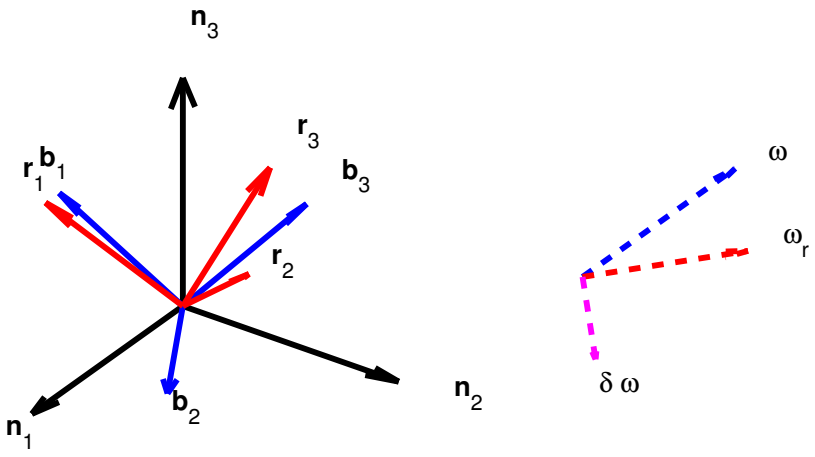

Figure 2.1: Tracking Control Coordinate Frames

The $\boldsymbol{\sigma}_\delta$ notation is chosen over the more obvious $\delta\boldsymbol{\sigma}$ to avoid any implication that it is simply a vectorial difference. The angular velocity error is defined in terms of the reference angular velocity $\boldsymbol{\omega}_r$ and body angular velocity $\boldsymbol{\omega}$ as

$$\delta\boldsymbol{\omega} = \boldsymbol{\omega} - \boldsymbol{\omega}_r \tag{2.18}$$

The candidate Lyupanov function here is

$$V = \frac{1}{2}\delta\boldsymbol{\omega}^T [I]\, \delta\boldsymbol{\omega} + 2K \ln\left(1 + \boldsymbol{\sigma}_\delta^T \boldsymbol{\sigma}_\delta\right) \tag{2.19}$$

This energy-like function is positive definite in terms of angular velocity and attitude error (a necessary condition to drive both errors to zero). Taking the inertial derivative of Eqn. (2.19) yields

$$\dot{V} = \delta\boldsymbol{\omega}^T \left([I] \frac{{}^{\mathcal{B}}\mathrm{d}}{\mathrm{d}\,t}\delta\boldsymbol{\omega} + K\boldsymbol{\sigma}_\delta \right) \tag{2.20}$$

As above, to ensure that this function is negative definite, it is set equal to

$$\dot{V} = -P\delta\boldsymbol{\omega}^T \delta\boldsymbol{\omega} \tag{2.21}$$

Selection of positive scalar gain P ensures that the function is negative semidefinite. Setting Eqns.

(2.20) and (2.21) equal results in the following conditions

$$[I]\frac{^{\mathcal{B}}\mathrm{d}}{\mathrm{d}\,t}\delta\boldsymbol{\omega} + P\delta\boldsymbol{\omega} + K\boldsymbol{\sigma}_{\delta} = \mathbf{0} \tag{2.22}$$

Since Eqn. (2.21) is expressed in terms of the body frame derivative $\frac{^{\mathcal{B}}\mathrm{d}}{\mathrm{d}\,t}\delta\boldsymbol{\omega}$, it cannot be directly substituted into the governing equation of motion per se. $\delta\boldsymbol{\omega}$ is explicitly expressed in the body frame $\mathcal{B}$ for any useful attitude control application, and derivatives are taken implicitly in the body frame as well. However, this quantity can easily be related to the actual inertial derivative seen in Eqn. (2.11) by applying the transport theorem

$$\frac{^{\mathcal{B}}\mathrm{d}}{\mathrm{d}\,t}\delta\boldsymbol{\omega} = \dot{\boldsymbol{\omega}} - \dot{\boldsymbol{\omega}}_r + \boldsymbol{\omega}\times\boldsymbol{\omega}_r \tag{2.23}$$

Utilizing this relationship and substituting Eqn. (2.22) into Eqn. (2.11) yields the following tracking control law, which is also applied in the simulations below

$$[G]\,\mathbf{u} = K\boldsymbol{\sigma} + P\delta\boldsymbol{\omega} - [\tilde{\omega}]\left([I]\,\boldsymbol{\omega} + [G]\,\mathbf{h}_s - \boldsymbol{\omega}_r\right) - [I]\left(\dot{\boldsymbol{\omega}}_r - [\tilde{\omega}]\,\boldsymbol{\omega}_r\right) \tag{2.24}$$

This control now guarantees that the attitude and velocity errors will be driven to zero.

Chapter 3

Power Optimal Control Development

3.1 Mathematical Approach

Based upon the current spacecraft state, the reaction wheel control laws above (as well as any similar law) specify the control torque $\mathbf{L}_r$, defined as

$$\mathbf{L}_r = [G]\,\mathbf{u} \tag{3.1}$$

at all times. Note that this is a projection of the internal wheel torques onto the body torque space, but not an external torque. Two properties are apparent from Eqn. (3.1). First, it is apparent that the wheel orientation vectors $\hat{\mathbf{g}}_i$ must span three-dimensional space in order to generate an arbitrary control torque, so $[G]$ must generally be full rank. Additionally, if there are more than three wheels, this system is underdetermined (a higher dimensional vector space projected onto a lower dimensional space), and has an infinite number of solutions.

After the desired control torque $\mathbf{L}_r$ is known, it is then necessary to find the combination of wheel torques u_i which generates this result. One possible solution to Eqn. (3.1) is the minimum norm torque, $\mathbf{u}^*$. This is the projection of the wheel torque vector onto the control torque space which minimizes its L_2 norm[19]

$$\mathbf{u}^* = \left([G]^T\,[G]\right)^{-1}[G]^T\,\mathbf{L}_r \tag{3.2}$$

This solution is not only useful mathematically but also popular for practical application, since wheel motor torques are often a limiting factor, particularly for larger spacecraft.

Since the $\mathbf{L}_r$ torque product is determined by the control law, instantaneous optimal behavior is achieved by altering the solution for the wheel torque vector $\mathbf{u}$. As described above, $\mathbf{u}^*$ is only one possibility out of an infinite number of wheel torque solutions. All other solutions to Eqn. (3.1) are expressed as

$$\mathbf{u} = \mathbf{u}^* + \mathbf{u}_s \tag{3.3}$$

The supplementary torque vector $\mathbf{u}_s$ must be chosen carefully to avoid altering the control behavior. Since $\mathbf{u}$ must result in the same control torque (so that the behavior of the original control is not affected), the supplementary torque vector $\mathbf{u}_s$ must be in the null space of $[G]$ such that

$$[G]\,\mathbf{u}_s = \mathbf{0} \tag{3.4}$$

Because the supplementary torque vector $\mathbf{u}_s$ exists in the null space of $[G]$, it is expressed as a linear combination of the null space basis vectors, which is to say that

$$\mathbf{u}_s = \sum_{i=1}^{m} \tau_i\,\hat{\mathbf{n}}_i \tag{3.5}$$

The m dimensional null space is defined in terms of the n dimensional vectors $\hat{\mathbf{n}}_i$. Physically, these basis vectors define ratios in which torque can be applied to individual wheels such that a zero net control torque results. Note that since the wheel orientation vectors in $[G]$ are constant, so are the null space basis vectors. This is convenient when implementing the controls below, since it saves significant computational time. By defining the null space scaling vector $\boldsymbol{\tau}$ and null space matrix $[N]$ as

$$\boldsymbol{\tau} = \begin{pmatrix} \tau_1 \\ \tau_2 \\ \vdots \\ \tau_m \end{pmatrix} \tag{3.6}$$

$$[N] = \begin{bmatrix} \hat{\mathbf{n}}_1 & \hat{\mathbf{n}}_2 & \cdots & \hat{\mathbf{n}}_m \end{bmatrix} \tag{3.7}$$

the supplementary torque vector can be expressed compactly as

$$\mathbf{u}_s = [N]\,\boldsymbol{\tau} \tag{3.8}$$

Any value of $\boldsymbol{\tau}$ chosen will now result in the same control torque $[G]\,\mathbf{u}$, and this null space scaling vector is used as the free parameter when developing the optimal controls below. By this method, the attitude control and supplementary torques can be effectively decoupled, allowing for considerable freedom to achieve optimal behavior.

3.2 Review of Alternate Power Optimal Controls

This mathematical groundwork can be applied to obtain desirable optimal wheel torque solutions for any given general control law. An instantaneous L_2 power optimal control, which is the basis for the original work below, was derived by Schaub and Lappas[8], and is described briefly here.

To determine the power used by the wheel motors at any instant, the total system kinetic energy is first expressed as

$$K = \frac{1}{2}\boldsymbol{\omega}^T\,[I]\,\boldsymbol{\omega} + \frac{1}{2}J\sum_{i=1}^{n} J_i\left(\Omega_i + \omega_{s,i}\right)^2 \tag{3.9}$$

Taking the derivative, or applying the work-energy theorem[2], yields the following general expression for total wheel power in the absence of an external torque

$$P = \sum_{i=1}^{n} \Omega_i u_i \tag{3.10}$$

However, in a traditional system, power is required to accelerate or deccelerate the wheels. The power for such a system is then the product of the wheel speed and torque magnitudes only, regardless of direction, such that

$$P = \sum_{i=1}^{n} |\Omega_i u_i| \tag{3.11}$$

Therefore, it is desirable to minimize the L_2 norm of the wheel powers.

By defining the vector $\mathbf{P}$ of all of the individual powers $\omega_i u_i$, a scalar power-squared cost function is defined as

$$J = \frac{1}{2}\mathbf{P}^T\mathbf{P} \tag{3.12}$$

Substituting Eqn. (3.10) and defining $[\Omega] = \text{diag}\,(\Omega_i)$ gives

$$J = \frac{1}{2}\left([\Omega]\,\mathbf{u}\right)^T\left([\Omega]\,\mathbf{u}\right) \tag{3.13}$$

Substituting Eqns. (3.3) and (3.8) into the cost function in Eqn. (3.13) results in the following expression to be minimized

$$J = \frac{1}{2}\left([\Omega]\left(\mathbf{u}^* + [N]\,\boldsymbol{\tau}\right)\right)^T\left([\Omega]\left(\mathbf{u}^* + [N]\,\boldsymbol{\tau}\right)\right) \tag{3.14}$$

For the purposes of instantaneous power optimal control, $\boldsymbol{\tau}$ is the only free parameter in the cost function, since $[N]$ is a constant, $\mathbf{u}^*$ is governed directly by the desired control torque, and $\boldsymbol{\Omega}$ is a function of the (arbitrary) instantaneous wheel state. Therefore, the two necessary conditions to minimize the cost function are $\frac{\partial J}{\partial \boldsymbol{\tau}} = \mathbf{0}$ and $\frac{\partial^2 J}{\partial \boldsymbol{\tau}^2} > \mathbf{0}$. Taking the derivative of Eqn. (3.14) and setting it to zero yields

$$[N]^T[\Omega]^2[N]\,\boldsymbol{\tau} = -\,[N]^T[\Omega]^2\,\mathbf{u}^* \tag{3.15}$$

Assuming that $[N]^T[\Omega]^2[N]$ is invertible, this expression can be solved for $\boldsymbol{\tau}$. There is the potential for a degenerate case in which $\boldsymbol{\Omega} = \mathbf{0}$, causing $[N]^T[\Omega]^2[N]$ to be rank-deficient (in fact, only m wheels must have nonzero spin rates to guarantee full rank). This case may be handled via an alternate formulation which is omitted here. Finally, the resulting supplementary torque vector $\mathbf{u}_s$ is

$$\mathbf{u}_s = -\,[N]\left([N]^T[\Omega]^2[N]\right)^{-1}[N]^T[\Omega]^2\,\mathbf{u}^* \tag{3.16}$$

This expression is substituted into Eqn. (3.3) to give the total wheel torque vector.

3.3 Regenerative Power Optimal Control

A similar methodology is applied to develop the regenerative power optimal control, so-called because power can be regenerated from the wheels (no norm is applicable here). Assuming perfect power return efficiency, the power required to generate this wheel torque at any given set of wheel speeds is simply the summation of the individual wheel powers. With this in mind, Eqn. (3.10)

can be expressed vectorially as

$$P = \mathbf{\Omega}^T \mathbf{u} \tag{3.17}$$

Substituting Eqn. (3.3) and Eqn. (3.8) into the power equation gives the following regenerative power cost function

$$P = \mathbf{\Omega}^T \left(\mathbf{u}^* + [N] \boldsymbol{\tau} \right) \tag{3.18}$$

At any arbitrary instant in time, $\mathbf{\Omega}$ is a function of the instantaneous state and cannot be altered. Similarly, $\mathbf{u}^*$ is a function only of the instantaneous state, and $[N]$ is a constant. The power is then only a function of the null space vector $\boldsymbol{\tau}$. Since $\boldsymbol{\tau}$ is the only free parameter, Eqn. (3.18) is linear function representing an $m+1$ dimensional hyperplane, the slope of which is a function only of the wheel geometry and wheel speeds.

Since the function is linear, the direction of the power extrema at any point can be found by taking the gradient of this plane, keeping in mind that all terms except $\boldsymbol{\tau}$ are fixed.

$$\nabla P = \frac{\partial P}{\partial \boldsymbol{\tau}} = \mathbf{\Omega}^T [N] \tag{3.19}$$

The extrema of the power plane lie along the gradient direction, so the extremizing null space vector $\boldsymbol{\tau}_s$ can be expressed in terms of the gradient (and m dimensional vector in the null space) and an unknown scalar multiplier α

$$\boldsymbol{\tau}_s = \alpha \nabla P^T = \alpha \left[N \right]^T \mathbf{\Omega} \tag{3.20}$$

$\boldsymbol{\tau}_s$ is a column vector, so ∇P is transposed since the result of Eqn. (3.19) is a $1 \times m$ matrix containing the gradient vector elements. This geometry is shown in the null space (for an $m = 2$ case) in Fig. (3.1).

With the extremizing null space vector $\boldsymbol{\tau}_s$ defined in Eqn. (3.20), the corresponding extremizing supplementary wheel torque vector $\mathbf{u}_s$ can be found from Eqn. (3.8).

$$\mathbf{u}_s = \alpha \left[N \right] \boldsymbol{\tau}_s \tag{3.21}$$

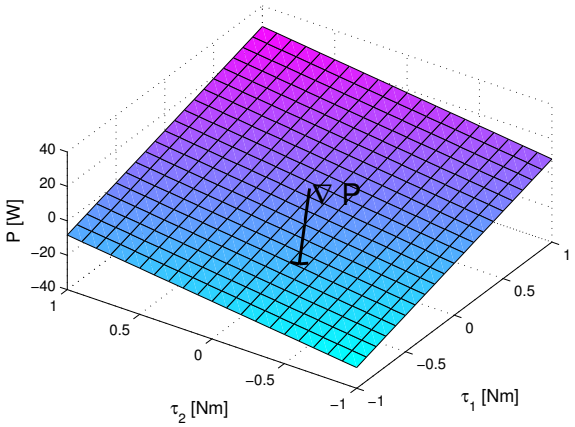

Figure 3.1: Power Hyperplane and Gradient in Null Space of $[G]$

Finally, substituting the definition of $\boldsymbol{\tau}_s$ in Eqn. (3.20) gives the following expression for $\mathbf{u}_s$ in terms of the unknown scalar α

$$\mathbf{u}_s = \alpha \, [N] \, [N]^T \, \boldsymbol{\Omega} \tag{3.22}$$

It can be seen in Eqn. (3.21) that $\mathbf{u}_s$ is an n-dimensional line in the power function gradient direction. The scalar multiplier α must then be chosen to maximize the magnitude of $\mathbf{u}_s$, thereby maximizing the change in power use. However, based on this information alone, the power extrema appear to lie at $\alpha = \pm\infty$. This is logically consistent, since applying an infinite torque to accelerate a wheel would require infinite power, and stopping the wheel with infinite negative torque would return infinite power according to Eqn. (3.17). This is neither physically possible nor desirable, so the magnitude of $\mathbf{u}_s$ must be maximized subject to a set of constraints. These constraints are the physical limits on the wheel motor torques. Given that i^{th} motor can exert a maximum torque of $B_{h,i}$ and a minimum (negative direction) torque of $B_{l,i}$, each wheel torque u_i must satisfy

$$B_{l,i} \leq u_i \leq B_{h,i} \tag{3.23}$$

Each torque bound creates two bounding hyperplanes at $u_i = B_{l,i}$ and $u_i = B_{h,i}$. It can be assumed for most motors that $B_{h,i} = B_{l,i}$, but the separate values are preserved here for generality. At this point it becomes apparent that this is a saturated control problem. Since the resulting total wheel

torque vectors will always be intersecting with the cube, at least one motor torque will always be saturated.

The $2n$ values of α corresponding to each set of torque bound planes are calculated by finding the intersections of the gradient line with the bounding hyperplanes. For each pair of bounding planes, the points of intersection are found at

$$\begin{aligned} u_i^* + u_{s,i} &= B_{h,i} \\ u_i^* + u_{s,i} &= B_{l,i} \end{aligned} \tag{3.24}$$

By defining T_i as the i^{th} element of the $[N]\boldsymbol{\tau}$ torque space gradient vector and substituting Eqn. (3.21), Eqn. (3.24) becomes

$$\begin{aligned} u_i^* + \alpha T_i &= B_{h,i} \\ u_i^* + \alpha T_i &= B_{l,i} \end{aligned} \tag{3.25}$$

Rearranging gives the two α values for the i^{th} motor bounding hyperplane intersection with the low and high torque bounds, denoted $\alpha_{l,i}$ and $\alpha_{h,i}$, respectively.

$$\begin{aligned} \alpha_{l,i} &= \tfrac{B_{l,i} - u_i^*}{T_i} \\ \alpha_{h,i} &= \tfrac{B_{h,i} - u_i^*}{T_i} \end{aligned} \tag{3.26}$$

The wheel torque bounding planes and the corresponding gradient direction intersections are shown in Fig. (3.2) given a four wheel case ($m = 1$) with arbitrary wheel rates and arbitrary $\mathbf{L}_r$, showing the intersection with the plane corresponding to each potential α value. The four dimensional wheel torque space is projected onto two separate two dimensional planes for simple visualization.

The surface which satisfies all of these constraints then forms an n-dimensional hypercube, and the extrema of the cost function (the maximum supplementary torque vector magnitudes) are found at the intersection of $\mathbf{u}_s$ with this hypercube. If the minimum norm torque $\mathbf{u}^*$ satisfies the torque constraint, there are only two possible intersections of $\mathbf{u}_s$ with the bounding hypercube (this is a defining characteristic of a convex polyhedron such as a cube, regardless of dimension). This is a safe assumption, since a $\mathbf{u}^*$ which violated the torque constraints would no longer guarantee

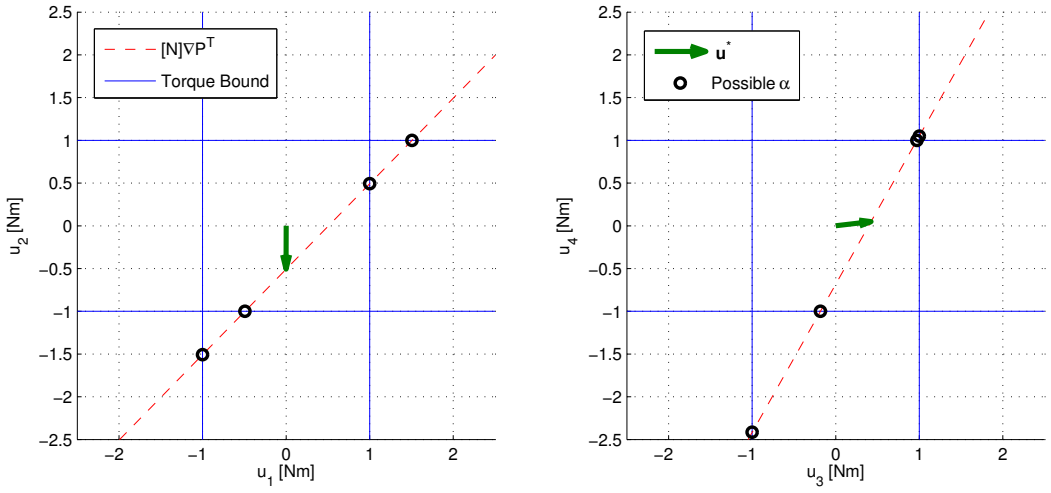

Figure 3.2: Gradient Line-Bounding Plane Intersection

stability and indicate a fundamental problem with the control gain selection. In practice, these two intersections are found by testing every possible $\alpha_{l,i}$ and $\alpha_{h,i}$ solution against every constraint. Figure (3.3) shows the two possible supplementary torque vectors which satisfy all of the constraints. In this example, it is apparent that the limiting torque hyperplanes (the sides of the hypercube

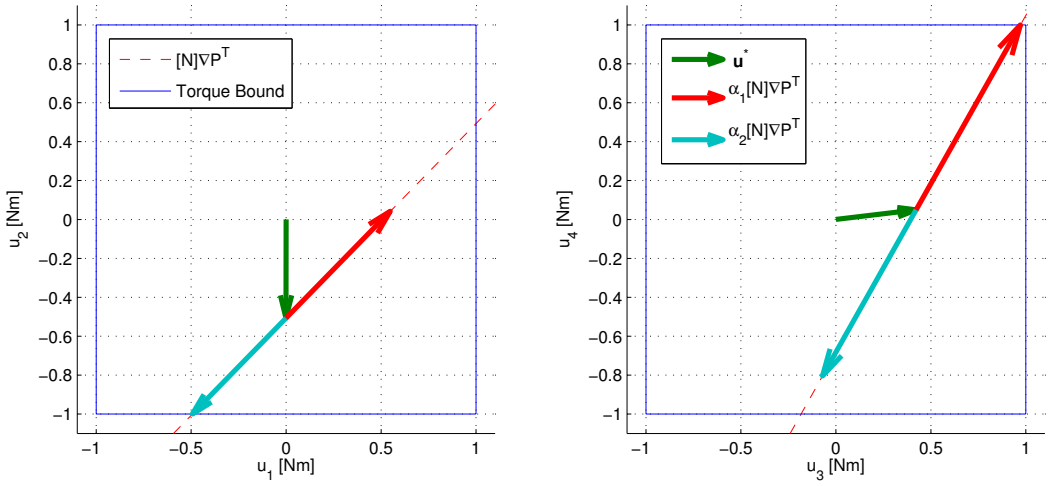

Figure 3.3: Supplementary Torque Vector-Hypercube Intersection

with which $\mathbf{u}_s$ intersects) are $u_2 = B_{l,2}$ and $u_4 = B_{h,4}$. When numerically implemented, it can be safely assumed that only two α values will be found, since more than two values can only occur

if $\mathbf{u}_s$ passes through an edge or corner of the hypercube (this is a result of testing the bounding planes individually), and a solution falling precisely on an edge or corner is very unlikely. Even in the event that this did occur, resulting in more than two possible α values, only two of the values would be distinct, and one of the repeated values could be selected arbitrarily. Only the distinct values $\alpha_{1,2}$ are dealt with below.

The resulting two α values now generate the maximum and minimum possible power use. Additionally, it is apparent from the geometry in Fig. (3.3) that $\alpha_1 \leq 0$ and $\alpha_2 \geq 0$, assuming that $\mathbf{u}^*$ satisfies the torque constraints. Since α_1 moves in the negative gradient direction and α_2 moves in the positive gradient direction, α_1 and α_2 correspond to the minimum and maximum power, respectively. This may be easily verified by substitution into the original power equation. From Eqns. (3.22) and (3.3), the wheel torque vector is

$$\mathbf{u}_{1,2} = \mathbf{u}^* + \alpha_{1,2} \left[N\right] \left[N\right]^T \mathbf{\Omega} \tag{3.27}$$

Substituting Eqn. (3.27) into Eqn. (3.18) gives

$$P_{1,2} = \mathbf{\Omega}^T \left(\mathbf{u}^* + \alpha_{1,2} \left[N\right] \left[N\right]^T \mathbf{\Omega} \right) \tag{3.28}$$

The product $\mathbf{\Omega}^T \left[N\right] \left[N\right]^T \mathbf{\Omega}$ is nonnegative scalar, confirming by inspection that $\max\left(\alpha_{1,2}\right)$ corresponds to $P_{\max}$ and $\min\left(\alpha_{1,2}\right)$ corresponds to $P_{\min}$. Selecting α_1 gives the final minimum power wheel torque as

$$\mathbf{u} = \mathbf{u}^* + \alpha_1 \left[N\right] \left[N\right]^T \mathbf{\Omega} \tag{3.29}$$

Like the other instantaneous power optimal control above, this can be applied to any control law generating an instantaneous desired $\mathbf{L}_r$ control torque.

Since α_1 and α_2 generate the minimum and maximum possible power solutions, any α satisfying

$$\alpha_1 \leq \alpha \leq \alpha_2 \tag{3.30}$$

is also admissible. According to Eqn. (3.28), power varies linearly with α, so a range of wheel motor total powers between P_1 and P_2 is available at any instant, as shown in Fig. (3.4). This

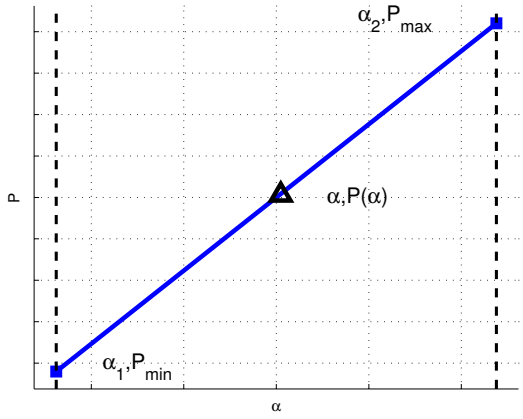

Figure 3.4: Instantaneous Power Range

property is useful to modify the control's power behavior, and the potential application for power tracking and IPACS is discussed further below.

3.4 Numerical Implementation

While control formulation presented above is free of mathematical singularities, there are numerical issues which must be dealt with. As the excess system energy approaches zero, the power hyperplane in Eqn. (3.18) flattens and the gradient approaches $\mathbf{0}$. As the norm of the gradient becomes critically small, machine roundoff error begins to dominate the gradient vector, causing rapid changes in ∇P and corresponding sign changes in the two α solutions. The resulting chatter behavior, shown below, is undesirable for any practical application, even though the resulting control torque is unaffected. Not only would this create unnecessary mechanical stresses, but such oscillations would be more likely to excite undesirable elastic modes in the spacecraft[5]. Note that the wheels oscillate between the saturated torques at $\pm 1\,\mathrm{Nm}$. Since the regenerative control is always saturated, it can be thought of as a type of bang-bang control law. As such, this behavior can easily be alleviated by adding a deadband under which α_1 is set to zero. This is easily implemented by using the magnitude of ∇P as the relevant scalar measure to which the deadband can be applied.

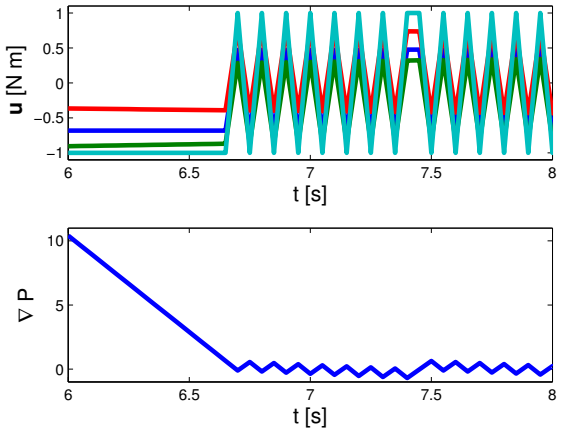

Figure 3.5: Wheel Torque Chatter

Using the deadband value ϵ, this is expressed as

$$|\nabla P| < \epsilon \implies \alpha_1 = 0 \tag{3.31}$$

The effect of implementing the deadband is shown in Fig. (3.6). The resulting motor torques

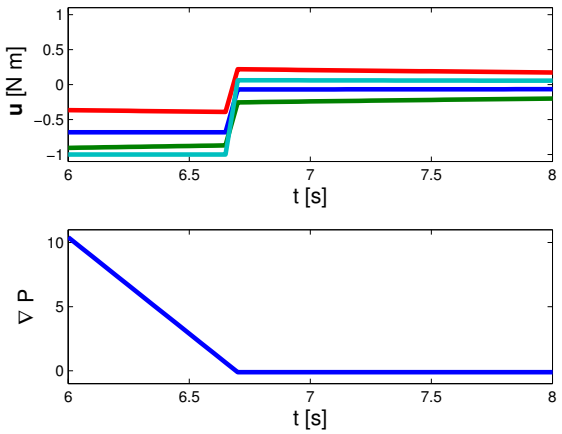

Figure 3.6: Chatter Removal Using $\epsilon = 0.3$ Deadband

are much better behaved, with the violent oscillations completely removed. The selection of ϵ is somewhat arbitrary, but may be set to a relatively large value ($\epsilon = 0.3$ is used above) since it has little impact on power performance and total energy return. For example, in the configuration used above, increasing the deadband by and order of magnitude from $\epsilon = 0.3$ to $\epsilon = 3$ engages the

deadband 0.2 seconds earlier, and only reduces the total energy returned by 0.3 J.

Chapter 4

Numerical Simulations

4.1 System Definition

The simulations below are performed with a 4-wheeled craft, with an inertia of

$$\text{diag}\ (5, 5, 8)\ \text{kg} \cdot \text{m}^2$$

The reaction wheels all have a spin axis inertia of $J_i = 0.1\,\text{kg} \cdot \text{m}^2$. The torque boundary for all wheel motors is $B_{h,i} = -B_{l,i} = 1\,\text{Nm}$. Two different sets of spacecraft initial angular velocities and wheel speeds are used, each chosen to accentuate different behavior characteristics. Initial State A has perturbed angular velocity (for the velocity regulation simulations), and Initial State B has a perturbed initial attitude and angular velocity (for the tracking control simulations).

Initial State A	$\boldsymbol{\sigma}_0 = \mathbf{0},\ \boldsymbol{\omega}_0 = \begin{bmatrix} 0 & 1 & 2 \end{bmatrix}^T$ rpm, $\boldsymbol{\Omega}_0 = \begin{bmatrix} 500 & 500 & 500 & 200 \end{bmatrix}^T$ rpm
Initial State B	$\boldsymbol{\sigma}_0 = \begin{bmatrix} 0 & 0.5 & 0.2 \end{bmatrix}^T,\ \boldsymbol{\omega}_0 = \mathbf{0}$ rpm, $\boldsymbol{\Omega}_0 = \begin{bmatrix} 500 & 500 & 500 & 500 \end{bmatrix}^T$ rpm

The four wheels are arranged in a "tripod" configuration, shown in Fig. (4.1). This is a popular redundant wheel configuration, since the fourth wheel can be used to generate an arbitrary three axis control torque in the event that any of the first three orthogonal wheels fails. The corresponding $[G]$ for this geometry is

$$[G] = \begin{bmatrix} 1 & 0 & 0 & -1/\sqrt{3} \\ 0 & 1 & 0 & -1/\sqrt{3} \\ 0 & 0 & 1 & -1/\sqrt{3} \end{bmatrix} \tag{4.1}$$

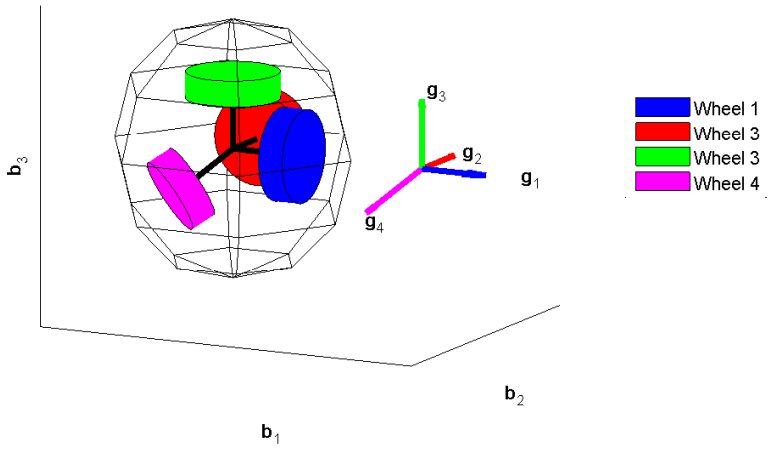

Figure 4.1: Tripod Wheel Configuration

Since this configuration has four wheels ($n = 4$), there is a one-dimensional null space ($m = 1$). To satisfy Eqn. (3.4), the $[G]$ matrix multiplied by any linear combination of the null space basis vectors must equal the zero vector $\mathbf{0}$. With this in mind, the basis vector may be calculated as follows, using a, b, c, and d as the components of the unknown basis vector.

$$\begin{bmatrix} 1 & 0 & 0 & -1/\sqrt{3} \\ 0 & 1 & 0 & -1/\sqrt{3} \\ 0 & 0 & 1 & -1/\sqrt{3} \end{bmatrix} \begin{bmatrix} a \\ b \\ c \\ d \end{bmatrix} = \mathbf{0} \tag{4.2}$$

This system of equations can be solved by setting one of the variables (in this case d) as a free parameter, which gives

$$\begin{bmatrix} a \\ b \\ c \end{bmatrix} = \frac{d}{\sqrt{3}} \begin{bmatrix} 1 \\ 1 \\ 1 \end{bmatrix} \tag{4.3}$$

Normalizing to $d = 1$ gives the following basis vector for the null space of $[G]$

$$\hat{\mathbf{n}}_1 = \begin{bmatrix} 1/\sqrt{3} \\ 1/\sqrt{3} \\ 1/\sqrt{3} \\ 1 \end{bmatrix} \tag{4.4}$$

This operation is equally applicable to higher dimensional null spaces, but becomes tedious when performed by hand and can easily be automated.

4.2 At-Rest Power Minimization

In this simulation the spacecraft is initially at rest, and the regulator control described in Eqn. (2.15) is implemented. The control law is unimportant for this simulation, since the initial angular velocity is zero, resulting in a control torque $\mathbf{L}_r$ that is always zero. Thus only null motion torques are applied to the wheels in order to return energy from them. The standard minimum norm regulator control $\mathbf{u} = \mathbf{u}^*$, which does not utilize any null motion and remains inactive, is included for a point of reference. The simulation begins at Initial State B.

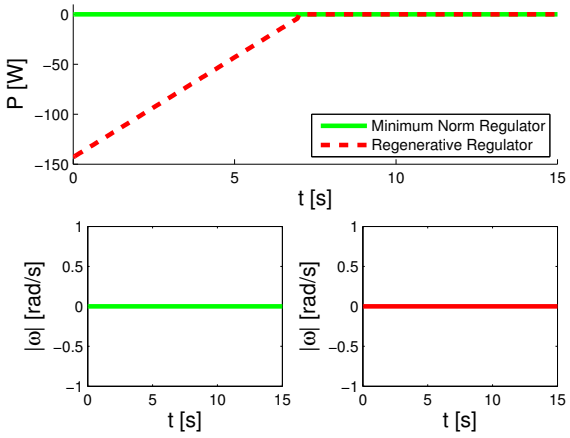

Figure 4.2: Regulator Control Power Comparison, $\boldsymbol{\omega}_0 = \mathbf{0}$

Fig. (4.3) shows the wheel rates over the duration of the simulations, which reach their steady state value as the return power goes to zero. Both controls keeps the spacecraft at rest, generating

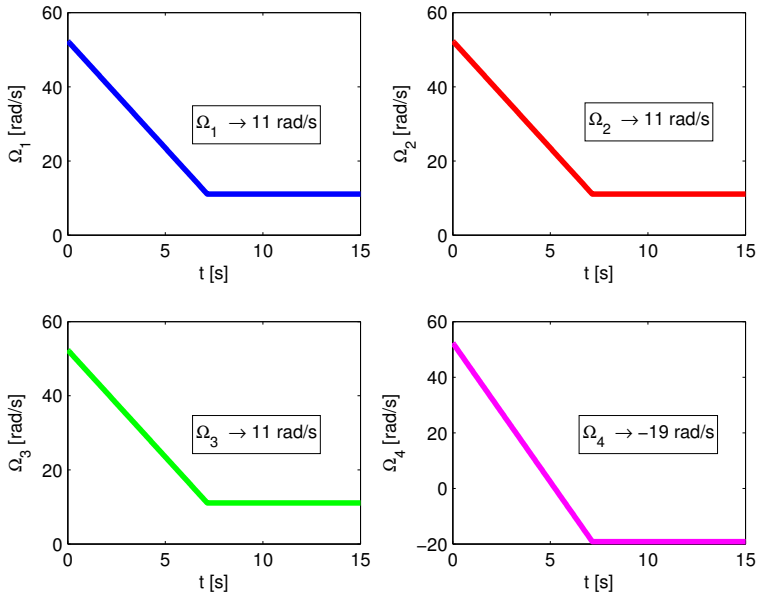

Figure 4.3: Regulator Control Wheel Speed Comparison, $\boldsymbol{\omega}_0 = \mathbf{0}$

zero net control torque. While the standard regulator applies no wheel torque, the regenerative regulator returns energy from the wheels. Since the goal of the wheel null motion is to extract the maximum amount of power from the wheels at all times, it follows that the wheels ought to reach their minimum energy state as $t \to \infty$. The minimum wheel speed can be calculated analytically by determining the minimum energy solution which satisfies conservation of momentum in the inertial frame.

Assuming that all of the wheels have the same inertia J, application of Eqn. (3.9) gives the following expression for the total kinetic energy K

$$K = \frac{1}{2}\boldsymbol{\omega}^T [I]\, \boldsymbol{\omega} + \frac{1}{2} J \sum_{i=1}^{4} (\Omega_i + \omega_{s,i})^2 \tag{4.5}$$

Using these terms, the spacecraft angular momentum is expressed as

$$\mathbf{H} = [I]\, \boldsymbol{\omega} + [G]\, \mathbf{h} \tag{4.6}$$

Given that the spacecraft is initially at rest with angular momentum $\mathbf{H_0} = \begin{bmatrix} h_1 & h_2 & h_3 \end{bmatrix}^T$, and using Eqn. (4.6) with the wheel configuration in Eqn. (4.1), the wheel speeds are related to

the initial angular momentum by

$$\begin{pmatrix} h_1 \\ h_2 \\ h_3 \end{pmatrix} = J \begin{pmatrix} \Omega_1 - 1/\sqrt{3}\Omega_4 \\ \Omega_2 - 1/\sqrt{3}\Omega_4 \\ \Omega_3 - 1/\sqrt{3}\Omega_4 \end{pmatrix} \tag{4.7}$$

Substituting this result into Eqn. (4.5) gives the following expression for total kinetic energy

$$K = J\frac{1}{2}\left(\left(\frac{h_1}{J} + \frac{1}{\sqrt{3}\Omega_4}\right)^2 + \left(\frac{h_2}{J} + \frac{1}{\sqrt{3}\Omega_4}\right)^2 + \left(\frac{h_3}{J} + \frac{1}{\sqrt{3}\Omega_4}\right)^2 + \Omega_4^2\right) \tag{4.8}$$

Because $\mathbf{H}_0$ remains constant in the absence of external torque, setting the derivative of Eqn. (4.8) to zero and solving for Ω_4 yields the following minimum energy wheel speeds

$$\begin{pmatrix} \Omega_1 \\ \Omega_2 \\ \Omega_3 \\ \Omega_4 \end{pmatrix} = -\frac{1}{J} \begin{pmatrix} \frac{h_2+h_3-5h_1}{6} \\ \frac{h_1+h_3-5h_2}{6} \\ \frac{h_1+h_2-5h_3}{6} \\ \frac{h_1+h_2+h_3}{\sqrt{12}} \end{pmatrix} \tag{4.9}$$

These results are somewhat more complex for the more general case of varying wheel inertias and nonzero spacecraft initial velocity, but the same analysis applies. Evaluating Eqn. (4.9) with the initial conditions given above gives the theoretical minimum wheel spin rates for this configuration.

$$\left.\begin{pmatrix} \Omega_1 \\ \Omega_2 \\ \Omega_3 \\ \Omega_4 \end{pmatrix}\right|_{\min(K)} = \begin{pmatrix} 11.06 \\ 11.06 \\ 11.06 \\ -19.17 \end{pmatrix} \text{rad/s} \tag{4.10}$$

As expected, all of the wheel rates in Fig. (4.3) approach the values predicted in Eqn. (4.10). At this point, the minimum energy state has been reached, and no power can be returned from the wheels. This minimum energy state seeking behavior is desirable from wheel speed management standpoint. However, due to potential wheel stickage issues, the zero wheel speed crossing may be undesirable for some systems.

4.3 Regulation Power Minimization

In this simulation, the spacecraft is given a substantial initial angular velocity, starting at Initial State A. The same regulator control in Eqn. [2.15] is implemented. Two other controls are shown for comparison: a minimum norm control (Eqn. (3.2)), and a L_2 power optimal control (Eqn. (3.16)). Both of the power optimal controls consume less power than the minimum norm

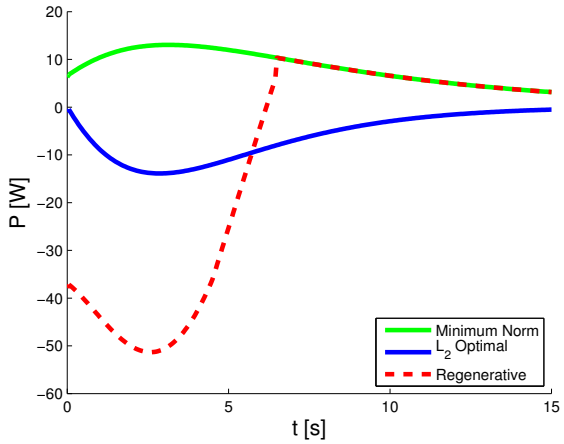

Figure 4.4: Regulator Control Power Comparison, Perturbed $\boldsymbol{\omega}_0$

control. While the regenerative regulator control returns considerably more power initially, it is eventually surpassed by the L_2 optimal control. This is a result of the fact that both controls only guarantee instantaneous power optimal behavior. As shown in Fig. (4.5), the two power optimal controls result in very different wheel rate time histories. This illustrates that while the regenerative control guarantees optimal power return for any instantaneous set of wheel rates, it is not necessarily superior to the L_2 optimal control at all points during the maneuver. However, the regenerative control can still be expected to extract more energy from the wheels for any given control torque history. This is confirmed by integration of the power histories; the L_2 optimal control returns 95.3 J, while the regenerative control returns 163.7 J.

The same minimum energy state seeking behavior seen in Fig. (4.2) is also seen for the nonzero inital spacecraft angular velocity. Fig. (4.6) shows the total system kinetic energy, as

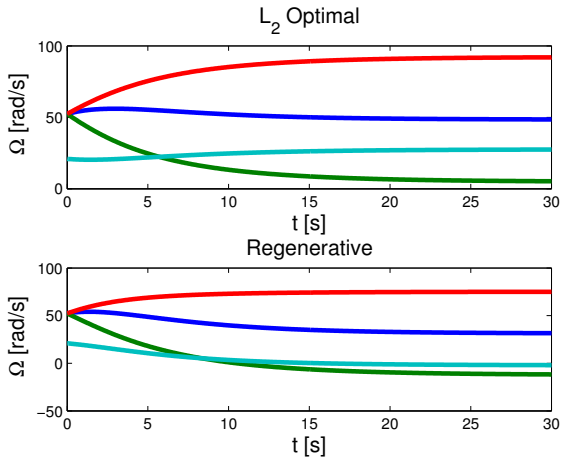

Figure 4.5: Power Optimal Control $\mathbf{\Omega}$ Comparison

calculated from Eqn. (3.9). Also, since the regenerative control is always saturated, higher wheel

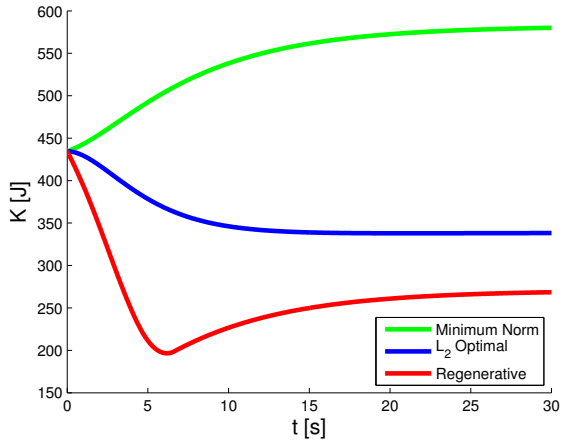

Figure 4.6: Total Kinetic Energy Comparison

torques are expected at all times. By definition, both of the power optimal controls will produce larger wheel torques than the minimum-norm control.

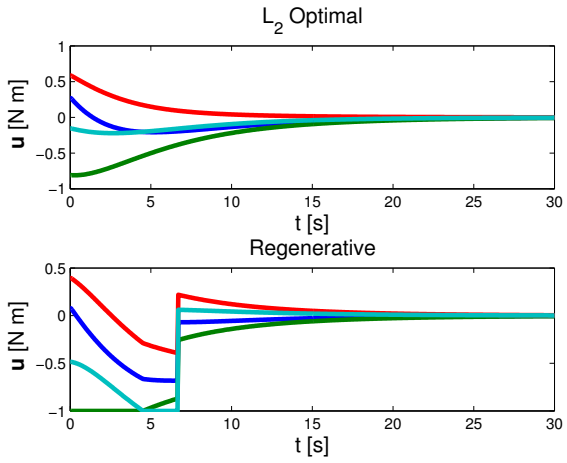

Figure 4.7: Power Optimal Control **u** Comparison

4.4 Tracking Power Minimization

While all of the controls above have been velocity regulators, the control law implemented below (Eqn. (2.24)) tracks a specific attitude and angular velocity profile, starting at Initial State B. The selected angular velocity error and attitude error gains are, respectively, $P = 1.2$ and $K = 0.3$. In Fig. (4.8) the minimum norm wheel torque solution is implemented, tracking the attitude history $\boldsymbol{\sigma}_r = \begin{bmatrix} 0.3\sin(0.02t) & -0.3\sin(0.02t) & 0 \end{bmatrix}^T$. The corresponding reference angular velocity is calculated by applying MRP kinematic relations to the easily differentiable attitude history, giving[2]

$$\boldsymbol{\omega}_r = \frac{1}{4}\left[\left(1 - \boldsymbol{\sigma}^T\boldsymbol{\sigma}\right)[I_{3\times3}] + 2[\tilde{\sigma}] + 2\boldsymbol{\sigma}\boldsymbol{\sigma}^T\right]^{-1}\dot{\boldsymbol{\sigma}} \tag{4.11}$$

As mentioned above, the selection of the wheel torque solutions does not affect the performance characteristics of the control, so the power optimal controls exhibit exactly the same behavior. The power behavior is much the same as seen in the regulator control above. Here the same control law is applied using the minimum norm, L_2 optimal, and regenerative wheel torque solutions. The 10 minute simulation is broken down into two segments illustrating different aspects of the response. Fig. (4.9) shows the first 30 seconds of the simulation. Exactly as seen in the velocity regulator control, the regenerative control initially returns a large amount of power as excess energy is removed

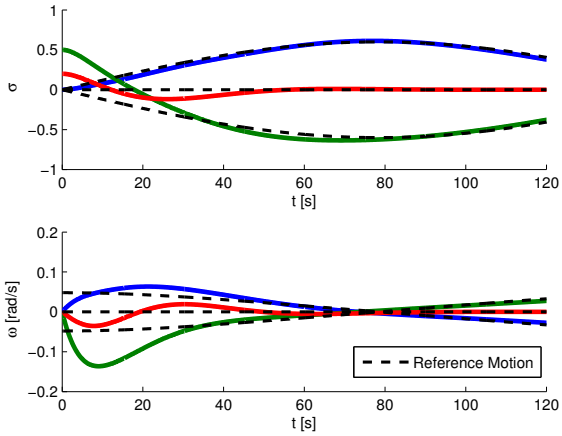

Figure 4.8: Minimum Norm Tracking Control

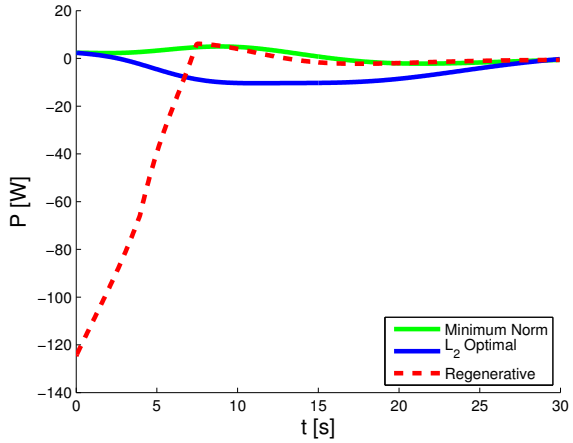

Figure 4.9: Power Comparison, 0 to 30 Seconds

from the system. Again, since both controls guarantee only instantaneous power optimality, neither can be said to always perform better than the other. Fig. (4.10) shows the remainder of the simulation, in which initial condition effects have largely vanished. Two behaviors are apparent here. First, the L_2 optimal control is no longer power optimal because of the altered power calculation; this was also the case in the regulator control above, but could not be illustrated since the control torque approached zero. Second, once it falls within the power plane gradient deadband, the regenerative power optimal control behaves identically to the minimum norm control.

To further understand the behavior of the three controls, it is useful to compare the evolution

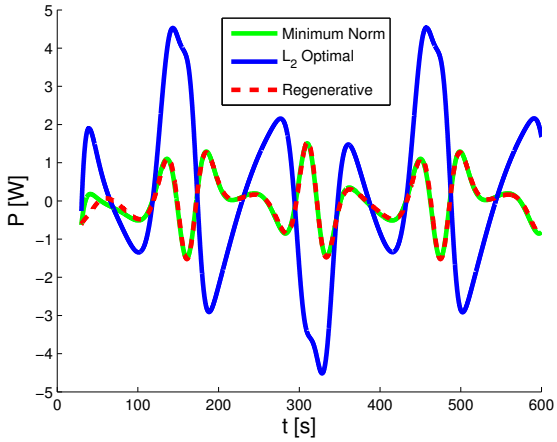

Figure 4.10: Power Comparison, 30 to 600 Seconds

of the total system energy as given in Eqn. (3.9). This is shown in Fig. (4.11). Since torque is

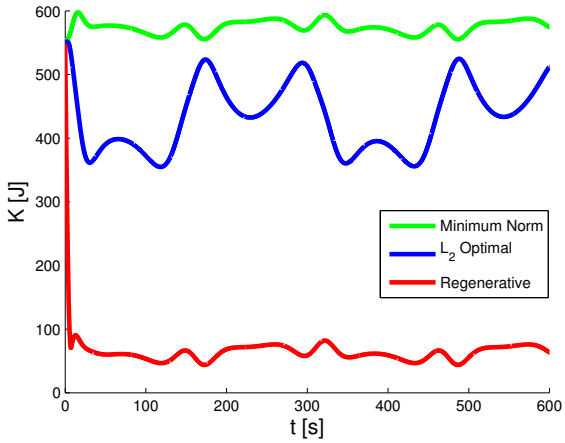

Figure 4.11: Total Kinetic Energy Comparison

applied to the system, energy is no longer conserved, but the regenerative control still exhibits the minimum energy state seeking behavior explored above. This also explains the lack of power optimal performance from the L_2 optimal control seen in Fig. (4.10), since its wheel state behavior left the system at a much higher total energy.

Chapter 5

Future Work and Conclusions

5.1 Future Work

5.1.1 Incorporation of Non-Unity Energy Return Efficiency

In a system which incorporates a system that returns energy from the reaction wheels, it can be safely assumed that this would not be done with perfect efficiency. This introduces the necessity for different efficiencies based upon the sign of the $\Omega_i \cdot u_i$ product, differentiating between acceleration and decceleration of the wheels. The resulting power function, using the power return efficiency $1-\eta$, is then

$$P = \mathbf{\Omega}^T \left(\left(1 - \frac{1}{2}\eta \right) [I_{3\times 3}] + \frac{1}{2}\eta \, \text{sign} \left(\mathbf{u}^* + [N]\, \boldsymbol{\tau} \right) \right) \left(\mathbf{u}^* + [N]\, \boldsymbol{\tau} \right) \tag{5.1}$$

The function is no longer continuously differentiable, and the methods above can only be applied locally, presenting a significant challenge.

5.1.2 Energy Storage

In addition to power optimal control, the power plane gradient concept can also be extended to formulation for a combined attitude control and energy storage system control. Based on Eqn. (3.28), the solutions for not only the instantaneous minimum power, but also the instantaneous maximum power are known. By selecting and α along the gradient direction that lies between the two extrema values, the full power input and output range allowed by the instantaneous state

and torque bounds can be utilized (as shown in Fig. (3.4)). An implementation which tracks an arbitrary power history, essentially very similar to that developed by [4], is shown below.

Since the relationship $P(\alpha)$ is linear, the α value which will generate any desired power P_t that lies within the instantaneous power boundaries can be trivially calculated as

$$\alpha_t = \frac{\alpha_{min} - \alpha_{max}}{P_{min} - P_{max}} (P_t - P_{min}) + \alpha_{min} \tag{5.2}$$

Fig. (5.1) applies this relationship to track the power history $P_t = 10 \sin\left(\frac{\pi}{5} t\right)$ W while performing simultaneous angular velocity regulation, beginning at Initial State A.

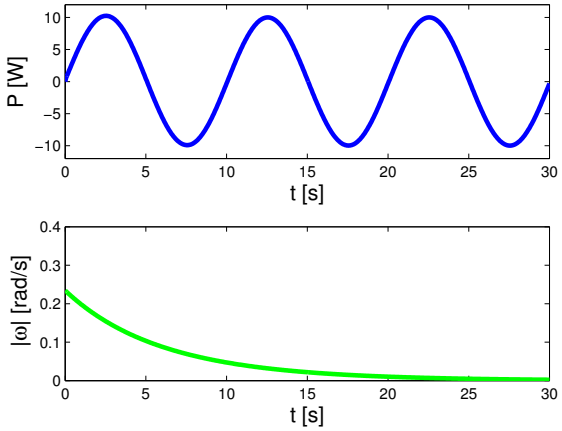

Figure 5.1: Power Tracking

It is also straightforward to generate the instantaneous power bounds over the course of the maneuver by application of Eqn. (3.28), and their resulting time histories are shown in Fig. (5.2). The necessity for imposing constraints on the desired power history is to be expected, since it is analogous to satisfying the wheel torque constraints on any general attitude control to ensure stability. Since any power profile desired from an IPACS over the course of the maneuver must lie within these bounds, this is potentially useful for generating these constraints for other integrated attitude control and energy storage strategies[12][15][16].

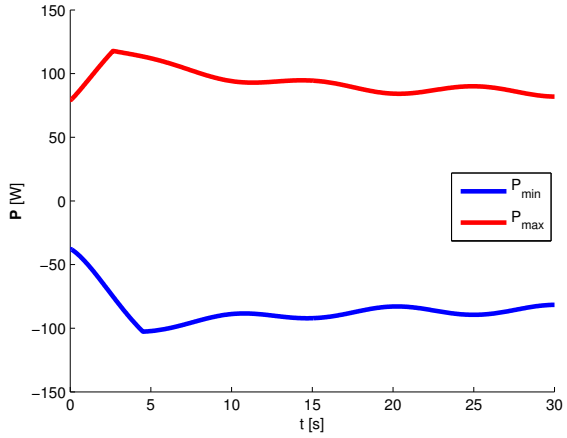

Figure 5.2: Min/Max Instantaneous Power Bounds

5.2 Conclusions

The control law developed above provides a method to minimize instantaneous power use for a redundant reaction wheel attitude control system utilizing flywheels for energy return. By expressing the total power to a linear function of the reaction wheel torque null space, the optimal wheel torque is determined analytically by application of constraints on the possible wheel motor torques, resulting in a saturated control. The formulation is applicable to any number of redundant wheels in any arbitrary geometry (which spans three-dimensional space). A potential numerical issue, which results in undesirable motor chatter behavior often seen in similar saturated bang-bang control laws, is eliminated by application of a simple deadband strategy.

The numerical simulations performed demonstrated a variety of control behaviors. The control was demonstrated to have identical attitude control performance to traditional wheel torque solutions as well as an L_2 power optimal control, while demonstrating favorable power optimal characteristic. An important behavior demonstrated throughout the simulations was the minimum energy state seeking, by which all excess energy is returned from the wheels, providing desirable power return and wheel speed management. This control was demonstrated to be valuable when optimal power behavior is desired from integrated energy storage and power tracking systems (par-

ticularly after incorporation of power return inefficiency), and also useful for characterizing the behavior of such integrated systems.

Bibliography

[1] James L. Wertz Wiley H. Larson, editor. Space Mission Analysis and Design. Microcosm Press, 1999.

[2] H. Schaub J. Junkins. Analytical Mechanics of Space Systems. American Institute of Aeronautics and Astronoautics, Inc., 2009.

[3] L. Sarsfield. The Universe on a Shoestring: Small Spacecraft for Earth and Space Science. RAND Critical Technologies Institute, 1998.

[4] P. Tsiotras et al. Satellite attitude control and power tracking with energy/momentum wheels. Journal of Guidance, Navigation and Control, 1999.

[5] L.G. Kraige S.B. Skaar. Large-angle spacecraft attitude maneuvers using an optimal reaction wheel power criterion. The Journal of the Astronautical Sciences, 32(1), 1984.

[6] D. J. Richie J. L. Fausz, editor. Flywheel Simultaneous Attitude Control and Energy Storage Using a VSCMG Configuration. Institue of Electrical and Electronics Engineers, 2000.

[7] M. Pastena M. Grassi. Minimum power optimal control of microsatellite attitude dynamics. Journal of Guidance, Navigation and Control, 23(5), 2000.

[8] V. Lappas H. Schaub. Redundant reaction wheel torque distribution yielding instantaneous l2 power-optimal attitude control. Journal of Guidance, Navigation and Control, 32(4), 2009.

[9] General Dynamics C4 Systems. Swift gamma-ray observatory performance characteristics, 2005. <http://www.gdc4s.com/documents/Swift_RevE.pdf>

[10] Goodzeit et al. Wheel speed management control system for spacecraft. U.S. Patent 5058835, 1991.

[11] Ratan et al. Optimal speed management for reaction wheel control system and method. U.S. Patent 7198232, 2007.

[12] C. D. Hall. High Speed Flywheels for Integrated Energy Storage and Attitude Control. American Control Conference, 1997.

[13] V. A. Spector T. J. Pieronek, D. K. Decker, editor. Spacecraft Flywheel Systems - Benefits, and Issues. Institue of Electrical and Electronics Engineers, 1997.

[14] M. R. Patel. Spacecraft Power Systems. CRC Press, 2005.

[15] J. W. Smay. Spacecraft energy storage, attitude steering, and momentum management system. U.S. Patent 5611505, 1997.

[16] Eisenhaure et al. Energy storage and attitude control reference system. U.S. Patent 4723735, 1988.

[17] Y. Choi et al. Efficient Control Torque Distribution Approach for Spacecraft Attitude Control. AIAA Guidance, Navigation, and Control Conference, 2008.

[18] Richie et al. Sizing/optimization of a small satellite energy storage and attitude control system. Major report, 2006.

[19] W. L. Brogan. Modern Control Theory. Prentice Hall, 1991.